Detection of Bearing Faults, using a Method that Combines Segmentation, Positive and Negative Signal Spectra, and Sparsity Measurements

Karim Bouaouiche

Electromechanical Engineering Laboratory, Electromechanical Department, Faculty of Technology, Badji Mokhtar-Annaba University, P.O. Box 12, Annaba, 23000, Algeria, e-mail: karim.bouaouiche@univ-annaba.dz

Abstract: *The spectrum of raw vibration signals is difficult to interpret because of the noise and useless information acquired during signal measurement. Consequently, several signal processing methods have been developed to improve diagnostic performance. These methods make it possible to obtain spectra with significant amplitude peaks. The comparison of the frequencies of these peaks with the theoretical frequencies of the faults, determined from mathematical equations, enables the faulty component to be identified. To simplify spectral representation and facilitate defection, a method based on determining positive and negative spectra is proposed. These spectra are obtained in several steps from the raw vibration signal. The signal is first segmented into several parts. Subsequently, the sparsity of each segment is measured using indices to select the dominant segment. The correlation between this dominant segment and all other segments is then assessed to identify those that contain similar information. The selected segments are denoised, using a wavelet-based method, and those lacking sufficient correlation, are replaced by a series of zeros. Then, the positive-negative spectrum method is applied. This method involves applying positive and negative thresholding to reconstruct two distinct signals: one containing positive values and the other containing negative values. A Fourier transform is applied to each of these two signals, yielding a simplified spectral representation that facilitates defect detection. Finally, applying the proposed method to signals from various databases, revealed high-amplitude peaks at frequencies characteristic of bearing defects, thereby demonstrating the efficacy in detecting failures.*

Keywords: bearing fault detection; vibration signal processing; positive and negative thresholding; sparsity measurement; fault frequencies.

1 Introduction

Bearings are organs used in industrial or automotive rotary equipment for the transmission of movements and the self-alignment of shafts. Thus, the bearing consists of a simple structure containing an inner and outer ring, cage, and rolling element, such as a ball or a conical or cylindrical roller. Defects in one of these components can cause a bearing or machine to malfunction. The sound and noise levels change during the fault creation process. Therefore, acoustic and vibrational analyses are important for the identification and localization of defects in rotating machinery and bearings [1]. In the industry, vibration analysis is more popular than other types of analysis because it incorporates several signal-processing methods to detect defects [1].

All diagnostic methods are based on extracting periodic impulse signals, caused by defects, that contain information directly related to the defect [2]. However, noise can cause difficulties during extraction [2]. Several data-extraction techniques exist, such as signal decomposition into several functions to separate data [3]. These functions are defined as useful or not using parameters such as the Gini index or energy [3]. Among the signal decomposition methods used in this context are Empirical Fourier Decomposition (EFD) [4] and the method developed by Nazari. M et al., called Successive Variational Mode Decomposition (SVMD) [5]. In addition, decomposition methods are integrated into signal denoising algorithms, such as the Donoho method, which consists of decomposition by transformation into discrete wavelets, with the use of a hard or soft threshold to eliminate noise [6]. Sahu P. K et al. proposed a method for detecting bearing defects [7]. The proposed method is based on denoising and envelope spectra [7]. The denoising method decomposes the data and implements an adaptive threshold to remove noisy components [7]. These components were selected based on correlation [7]. Detrended Fluctuation Analysis (DFA) is considered a step in some denoising methods, such as the method developed by Li.J et al. [8]. This method involves signal decomposition using a Variational Mode Decomposition (VMD) algorithm and scale parameter determination using detrended fluctuation analysis [8]. This parameter allows us to identify the type of noise, whether pink or white [8]. Once the noise type is defined for each component obtained after decomposition, the filtered signal is obtained by summing the noise-free components with scale parameter values that differ from those dependent on noise [8]. In addition, kurtosis is frequently used to identify defects in bearings [9]. This indicator takes a value greater than three for a failing bearing, whereas for a healthy bearing, it takes a value less than three [9]. Thus, it can be used for efficient signal reconstruction by identifying the pulses, caused by defects, using decomposition [9].

Deconvolution is an operation used in fault detection because it provides high performance for the extraction of fault-related pulses, whereas the vibration signal can be considered as the convolution product between the impulse signal and the transfer function between the fault source and the sensor [10]. Numerous methods have been developed in this context, such as fast nonlinear blind deconvolution proposed by Zhang.Z et al. [11]. Thus, envelope analysis, which consists of bandpass filtering and Hilbert transform, is an effective diagnostic tool [12]. Generally, most research in the field of envelope analysis focuses on the optimal selection of the frequency band for filtering using methods such as Autogram, which is based on unbiased autocorrelation [13]. The localization and identification of the failing components in a bearing are achieved by comparing the peak frequency of the envelope spectrum with the theoretical frequencies of the defects, which are determined by mathematical formulas [9]. However, the classification of defect types can be realized using a learning machine, which involves extracting features from the defect signals and inserting them into a classifier [14]. Thus, several diagnostic methods combine the decomposition and deconvolution of vibration signals.

Zhou, Yuquan et al. [15] proposed a method that combines Variational Mode Decomposition (VMD) and Maximum Correlation Kurtosis Deconvolution (MCKD) to extract defect characteristics. However, the input parameters of these two algorithms play a decisive role and strongly influence the performance of defect information extraction [15]. To address this limitation, the authors propose an optimization method based on Improved Singular Spectrum Analysis (ISSA) [15]. Similarly, Damine et al. [16] developed a method for detecting bearing defects based on the decomposition of the vibration signal using the Combined Modes Ensemble Empirical Mode Decomposition (CMEEMD) algorithm into several intrinsic mode functions (IMFs). Next, the Kurtosis Median Absolute Deviation (KMAD) indicator is used to select the optimal functions [16]. The selected components are then processed by the Improved Minimum Entropy Deconvolution (IMED) algorithm to reduce noise and improve the extraction of defect information [16]. Finally, the envelope spectrum is calculated to identify the characteristic frequencies of the defects [16].

In the same context, Xu Zhi et al. [17] proposed a method based on cascaded variational mode decomposition deconvolution designed to reduce the influence of noise on the detection of defect information. Building on this, we propose a diagnostic method that combines vibration signal decomposition, the selection of the most significant components using a newly developed indicator called the Defect Symptom (DS), and the use of the log-envelope spectrum to detect bearing defects [18]. In this review of the literature, it appears that existing work is primarily aimed at improving the extraction of fault information while reducing the effects of noise. However, most of these approaches rely on the use of the conventional envelope spectrum as a diagnostic tool. In response to this challenge, this paper proposes a new fault detection method based on a different spectral processing strategy. The main contributions and innovations of this study are as follows:

- A method for detecting defects is proposed. It is based on signal segmentation, impulsivity measurement, and a noise-reduction step that effectively eliminates noise, followed by the reconstruction of a new vibration signal containing primarily the information characteristic of the defects.

- Two new spectra, corresponding to the positive and negative signals, respectively, are developed from the positive and negative samples. These spectral representations, which are easier to interpret than the conventional envelope spectrum, facilitate the localization and identification of bearing defects.

The rest of the paper is organized as follows: Section (2) presents methods used in signal processing-based diagnostics; Section (3) illustrates the proposed methods; Section (4) outlines the application of the proposed method to experimental signals, and Section (5) illustrates the comparison of the diagnostic methods. Finally, in Section (6), conclusions are drawn.

2 Theoretical Background

2.1 Sparsity Measurement

The measurement of signal sparsity is carried out using indicators such as kurtosis, the Gini index, the Hoyer index, and the L2/L1 norm, which are defined by equations (1-4) [19], as well as negentropy, which is defined by equation (5) and enables the measurement of sparsity [20]. These indicators assess the impulsivity and energy concentration of the signal data [19]. Depending on the impulsivity, mechanical faults can be detected, as is the case for bearings: once kurtosis exceeds a value of three, the bearing is considered faulty [19]. However, according to reference [21], the Gini index performs better than kurtosis for measuring the number of pulses in a signal.

$$Kurtosis = \frac{\frac{1}{N}\sum_{n=1}^{N}\left(x_n - \bar{x}\right)}{\left(\frac{1}{N}\sum_{n=1}^{N}\left(x_n - \bar{x}\right)^2\right)} \tag{1}$$

$$L_2 / L_1 norm = \frac{\sqrt{\sum_{n=1}^{N} x_n^2}}{\sum_{n=1}^{N}\left|x_n\right|} \tag{2}$$

$$Hoyer \quad Index = \left(\sqrt{N} - \frac{\sum_{n=1}^{N} |x_n|}{\sqrt{\sum_{n=1}^{N} x_n^2}} \right) / \left(\sqrt{N} - 1 \right) \tag{3}$$

$$Gini \quad Index = 1 - 2 \sum_{n=1}^{N} \frac{x_n}{\|\vec{x}\|_1} \left(\frac{N - n + 0.5}{N} \right) \tag{4}$$

$$Negentropy = \frac{1}{N} \sum_{n=1}^{N} \left(\frac{x_n^2}{\frac{1}{N} \sum_{n=1}^{N} x_n^2} Ln \left(\frac{x_n^2}{\frac{1}{N} \sum_{n=1}^{N} x_n^2} \right) \right) \tag{5}$$

Where, (N and $\bar{x}$) represent the signal length and average, respectively, and $\|\vec{x}\|_1$ is the L1 norm.

2.2 Wavelet-based Denoising

Noise elimination using the Donoho algorithm, which is based on wavelet transform, consists of the following steps [22]:

- Decomposition of the signal into several components using discrete wavelet transform, whose coefficients are determined by the following equation:

  $$W_{j,k} = 2^{-j/2} \int_{-\infty}^{+\infty} x(t) \overline{\psi} \left(2^{-j} t - k \right) dt \tag{6}$$

  Where: (x) is the signal and ($\overline{\psi}$) is the conjugate complex of the mother wavelet (ψ).

- Application of a hard or soft threshold to the coefficients defined in equation (6). The hard and soft thresholds are defined as follows:

  $$Hard(W_{j,k}) = \begin{cases} W_{j,k} & |W_{j,k}| \geq \lambda \\ 0 & |W_{j,k}| < \lambda \end{cases} \tag{7}$$

$$Soft(W_{j,k}) = \begin{cases} sign(W_{j,k})(\left|W_{j,k}\right| - \lambda) & \left|W_{j,k}\right| \geq \lambda \\ 0 & \left|W_{j,k}\right| < \lambda \end{cases} \tag{8}$$

$$\lambda = \sigma\sqrt{2Log(N)} \tag{9}$$

Where: (σ) is the noise variance and (N) is the signal length.

- The inverse discrete wavelet transform is applied to the coefficients to obtain a high-quality noise-free signal in the time domain.

$$x(t) = \sum_{j=-\infty}^{+\infty} \sum_{k=-\infty}^{+\infty} W_{j,k} \times \psi_{j,k}(t) \tag{10}$$

Several parameters exist to evaluate the effectiveness of noise reduction methods, such as the Signal-to-Noise Ratio (SNR), which is defined by equation (11); therefore, this parameter has a high value for better noise suppression [23].

$$SNR = 10Log\left(\frac{S_p}{N_p}\right) \tag{11}$$

Where: (S_p)–power of the signal and (N_p)–power of noise.

2.3 Envelope Spectrum

The envelope spectrum is widely used as the final step in diagnostic methods, enabling frequency-based fault detection. This spectrum was obtained after applying the Fourier transform to the signal envelope and was extracted from the analytical signal defined by the Hilbert transform, as shown in equation (12) [24]. Therefore, the Taeger–Kaiser energy operator can be used to define the signal envelope, as illustrated in equation (13) [25].

$$\begin{cases} H[x(t)] = x(t) * \dfrac{1}{\pi t} \\ E(t) = \sqrt{x(t)^2 + H[x(t)]^2} \end{cases} \tag{12}$$

$$\begin{cases} TK[x(t)] = [\dot{x}(t)]^2 - x(t) \times \ddot{x}(t) \\ E(t) = \dfrac{2TK[x(t)]}{\sqrt{TK[\dot{x}(t)]}} \end{cases} \tag{13}$$

Where: ($H[.]$) – Hilbert transform, (E) – signal envelope, ($TK[.]$)–Taeger-Kaiser energy operator, ($\dot{x}$ and $\ddot{x}$) represent the first and second derivatives of the signal, respectively.

In addition, there are other types of envelopes, such as logarithmic and square envelopes. The generalized envelope defined by equation (14) can establish all these types [24]. In the case where parameter (P) in Eq. (14) is zero, we obtain the logarithmic envelope; for (P=2), we obtain the square envelope [24].

$$GE(t) = \begin{cases} Ln\left(E(t)\right) & P = 0 \\ E(t)^P & P > 0 \end{cases} \tag{14}$$

Next, the Fourier transform was used to determine the envelope spectrum, as outlined in equation (15) [24].

$$E(f) = \int_{-\infty}^{+\infty} E(t) \times e^{-j2\pi ft} dt \tag{15}$$

2.4 Bearing Fault Frequencies

Bearing component defects, such as those of the outer ring, inner ring, cage, and rolling element, are defined by frequency values that can be determined from mathematical formulas depending on the geometric parameters of the bearing and rotation speed during operation [18]. The defect frequencies of each bearing component are expressed in Hertz as follows [18]:

- Rolling element defect frequency (FRE)

$$FRE = \left(1 - \left(\frac{d}{D}\cos(a)\right)^2\right)\frac{Fr \times D}{2d} \tag{16}$$

- Cage fault frequency (FC)

$$FC = \left(1 - \frac{d}{D}\cos(a)\right)\frac{Fr}{2} \tag{17}$$

- Inner ring fault frequency (FIR)

$$FIR = \left(1 + \frac{d}{D}\cos(a)\right)\frac{z \times Fr}{2} \tag{18}$$

- Outer ring fault frequency (FOR)

$$FOR = \left(1 - \frac{d}{D}\cos(a)\right)\frac{z \times Fr}{2} \tag{19}$$

Where: (z) is the number of rolling elements, (a)–contact angle, (Fr)–rotation speed, (D)-pitch diameter and (d) is the diameter of the rolling element.

3 Proposed Methods

3.1 Positive and Negative Signal Spectrum

The proposed method, called positive and negative signal spectra, is used to simplify the shape of the vibration signal spectrum and make it easier to interpret because the original signal spectrum is complex. This method is intended to be used as a final step in fault detection to detect and identify faulty components based on high-amplitude peak frequencies. The spectrum of a positive or negative signal is determined by thresholding the raw signal as:

- For a vibration signal ($x = \{x_1, x_2, ..., x_N\}$), the average signal can be determined as follows:

$$M_i = \frac{x_i + x_{i+1}}{2} \quad i = 1,2,...,N \tag{20}$$

$$M = [M_1, M_2, ..., M_N] \tag{21}$$

Where (M) is the average signal of the raw signal data (x) along the length (N).

- Average signal data thresholding to determine and reconstruct two series: one containing positive samples and the other containing negative samples, using the following equations:

$$P_S[M_i] = \begin{cases} M_i & if \quad M_i > 0 \\ 0 & if \quad M_i \leq 0 \end{cases} \tag{22}$$

$$N_S[M_i] = \begin{cases} M_i & if \quad M_i < 0 \\ 0 & if \quad M_i \geq 0 \end{cases} \tag{23}$$

Where: (Ps) and (Ns) represent positive and negative thresholding, respectively.

- Fourier transform was applied to obtain the spectra of the positive and negative signals is expressed in equation (24):

$$S(f) = \int_{-\infty}^{+\infty} M \times e^{-j2\pi ft} dt \tag{24}$$

3.2 Fault Detection Method

Figure (1) shows a novel flowchart of the proposed fault detection method.

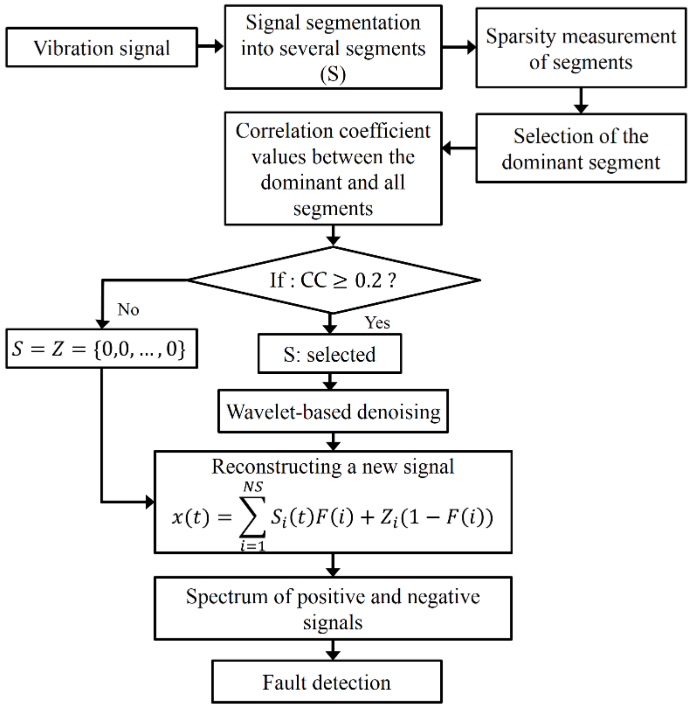

Figure 1
Flowchart of the fault detection method

The fault detection method comprises the following steps:

- **Step 1:** Segment the signal into several segments (S) using the buffer function in MATLAB. The number of segments is equal to the number of fault harmonics and is calculated by the following equation:

$$NS = \frac{F_S}{2F_d} \tag{25}$$

Where: (F_S) is the sampling frequency, (F_d) is the fault frequency, and (NS) represents the number of segments.

The number of segments must be integer and satisfy the condition expressed by equation (26). If dividing the raw signal length (N) by (NS) yields a fractional number, we perform a manual numerical approximation of the number of segments to obtain an integer.

$$\frac{N}{NS} = n \quad n = 1,2,\ldots,N \tag{26}$$

- **Step 2:** Measure segment sparsity using sparsity indices: kurtosis, L2/L1 norm, Hoyer index, Gini index and negentropy. The equations (1-5) respectively define these indexes. Once the values of the indexes are determined, a segment with high values for several indexes is selected as dominant.

- **Step 3:** Evaluate the correlation between the dominant segment and all segments using the correlation coefficient defined in equation (27) [7].

$$CC = \frac{Cov(S_d ; S)}{\sqrt{Var(S) \times Var(S_d)}} \tag{27}$$

  Where: (Cov) and (Var) represent covariance and variance, respectively, (S_d) represents the dominant segment.

  Correlation values between segments were generally low. However, segments with a correlation value greater than (0.2) were selected because they contained data that were slightly similar to that of the dominant segment.

- **Step 4:** Apply wavelet-based denoising to all segments selected in step 3 to eliminate noise and improve signal quality. Then, a vibration signal containing the defect data is constructed using a novel equation (28). This signal is equal to the sum of the dominant segments, whereas the non-dominant segments are replaced by a series of zeros of length identical to those of the original segments. A series of zeros replaced non-dominant segments to eradicate and lessen their influence on useful data.

$$\begin{cases} x(t) = \sum_{i=1}^{NS} S_i(t)F(i) + Z_i(1 - F(i)) \\ F(i) = 1 \quad if \quad \text{S : dominant} \\ F(i) = 0 \quad if \quad \text{S : non - dominant} \end{cases} \tag{28}$$

  Where: (S) is the signal segment at its position, (Z) is a series of zeros of the same length as segment, (x) is the new vibration signal.

- **Step 5:** Determining the spectrum of the positive or negative signal for detecting bearing faults based on a comparison between the frequencies of the high-amplitude peaks and the values of the fault frequencies of the bearing components, as determined by equations (16 thru 19).

4 Experimental Research

4.1 First Scenario

Ismail, M.A., et al., measured the vibration signals of a QJ212 TVP bearing from a vertically positioned test rig consisting of a motor and a spindle for mounting the bearing [26]. The load applied to the bearing was applied by a press, while the vibration acceleration was measured using an accelerometer model (PCB 356A32) positioned axially on the axis (x) of the bearing housing [26]. Bearing defects are of the spelling type and are identified by width (w), depth (d) and height (h) [26]. Defects are created by machining the inner and outer rings [26]. Additionally, an acquisition system collected the vibration signals and recorded them as MATLAB files at a sampling frequency of 25.6 kHz [26]. The bearing geometry and fault frequencies are given in Table (1) [26].

Table 1
Bearing geometry and fault frequencies

Pitch diameter	85.15 [mm]
Ball diameter	15.87 [mm]
Number of balls	15
Fault frequency of inner race	8.6427Fr [Hz]
Fault frequency of outer race	6.3573Fr [Hz]

The proposed method (Fig.1) is applied to the following signals [23]:

Table 2
Vibration signals

Signals	**Speed and load**	**Defect component**	**Fault frequency**
N5k_500_3.8_inner.mat	500 [Rpm], 5 [kN]	Inner race	72.0225 [Hz]
N8.8k_500_2.4_outer.mat	500 [Rpm], 8.8 [kN]	Outer race	52.9775 [Hz]

4.1.1 Results and Discussions

Case 1: Inner ring fault signal. The proposed fault detection method was applied to this case. The results of each step are shown as follows**:**

- According to equation (25), the number of segments is equal to (177), but this number does not satisfy the condition expressed by equation (26). Thus, we approximate the number of segments (NS) to (200). The variations in the sparsity index values are shown in figure (2). These values indicate that segment number (84) is dominant because it expresses high values for several indices.

- Segments of numbers NS = {9, 14, 34, 70, 75, 89, 109, 120, 125, 139, 159, 170, 184, 195}, which are efficient and contain data similar to the dominant segment, are selected. These segments express correlation values greater than (0.2), as shown in figure (3).

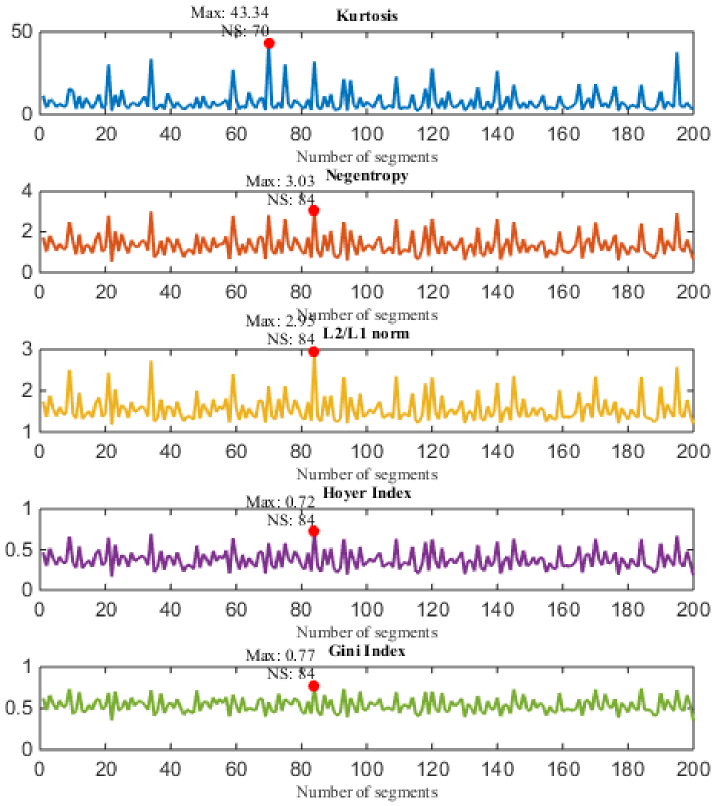

Figure 2

Sparsity indexes

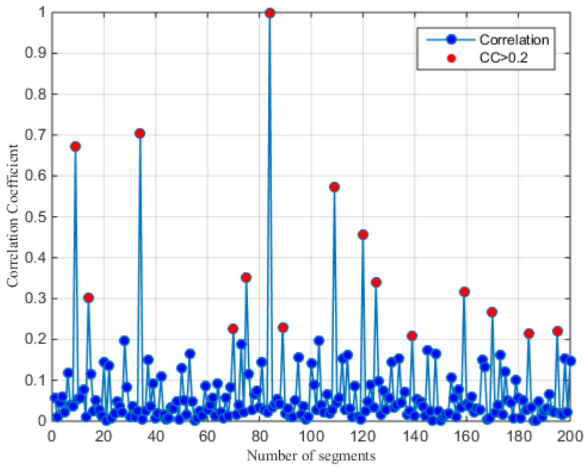

Figure 3
Correlation values

- Figure (4) shows the new signal obtained by Eq. (28). The SNR of this signal was equal to (0.211895 dB), with a highly reliable correlation value between the original signal and the new signal of (0.218219).

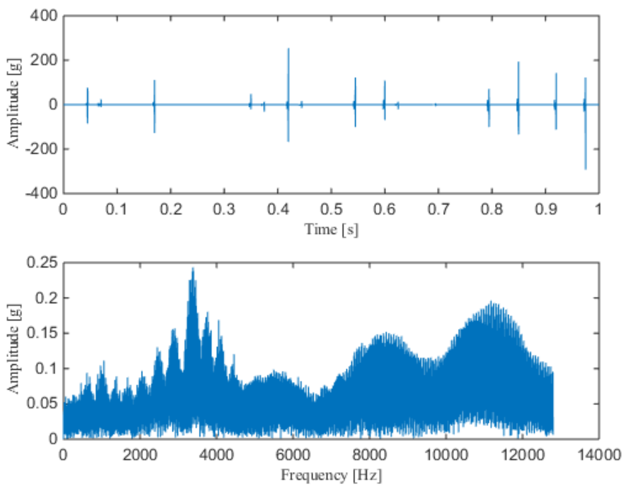

Figure 4
New signal

- In the spectrum of the positive and negative signals, high-amplitude peaks can be observed in the inner-ring fault frequency (72.0225Hz≈71.88 Hz), as shown in figure (5).

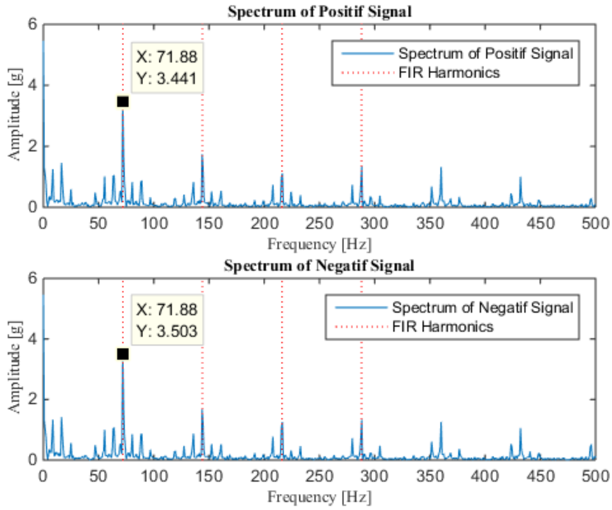

Figure 5

Spectrum of the positive and negative signals

Case 2: Outer ring fault signal. In this case, the signal is divided into (200) segments, and according to the sparsity index values, segment number (174) dominates. According to the correlation coefficient values, there were (36) significant segments. Then, after reconstructing the new signal and determining the spectrum of the positive and negative signals, a peak was observed in the outer ring fault frequency (53.13 Hz ≈ 52.9775 Hz), as shown in figure (6).

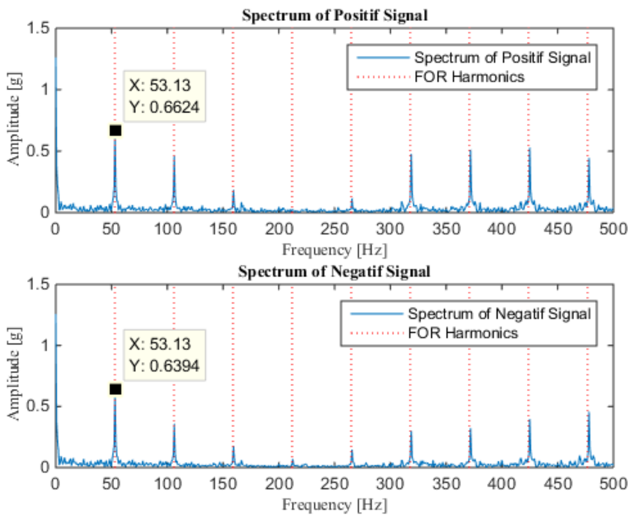

Figure 6

Outer ring fault detection

4.2 Second Scenario

Seongjae Lee et al., created a database of vibration signals for deep groove ball bearing (6204), cylindrical roller bearings (N204), and tapered roller bearing (30204) [27]. These signals were measured and collected from a test rig consisting of an electric motor and a shaft [27]. The end of the motor shaft was a bearing housing, followed by a rotor disc [27]. At the end of the disc, a bearing was positioned, and a PCB Piezotronics 333D01 accelerometer was mounted on a magnetic support to collect the vibration accelerations in units of gravitational [9.80665 m/s²] [27]. The accelerometer is connected to a laptop via USB. The signals were recorded as MATLAB files at sampling frequencies of 8 and 16 kHz [27]. In addition, the signals from the bearing positioned at the end of the rotor disc depend on other conditions, such as faults in rotating components: a loosening fault in the bearing located at the end of the motor, a misalignment fault in the motor's central axis, and a fault in the balance of the rotor disc [27]. Among all signals, we analyzed two signals presented in table (3) [27].

Table 3
Analyzed Vibration Signals

Signals	Rotating component condition	Defect component in bearing	Fault frequency [Hz]	Sampling frequency [kHz]
M1_OR_16_N204_600.mat	Misalignment	Outer race	42.86	16
U1_H_8_30204_1400.mat	Unbalance	Health	23.33	8

4.2.1 Discussions and Results

Situation 1: N204 bearing fault signal, when the motor's central shaft rotates with a misalignment fault. After analysis using the proposed method (Fig.1), the signal was divided into (200) segments, with the dominant segment being number (117). Then, after reconstruction of the new signal, in the spectrum of the positive and negative signals, the outer ring defect is detected on the basis of the large peak frequency (39.06 Hz≈42.86 Hz), and the misalignment is identified by the rotation frequency (2Fr ≈ 20 Hz), as shown in figure (7). The peak of misalignment was low because a fault was created at the electric motor, and the vibration signal was collected using an accelerometer mounted in the bearing, which was positioned at the end of the rotor disc.

Situation 2: The spectrum of the positive and negative signals on the rotor disk balance fault signal with a healthy bearing (30204), shown in figure (8), illustrates a train of peaks with high amplitudes of the rotation frequency (Fr=1400/60=23.33 Hz), and this peak reflects the presence of an imbalance.

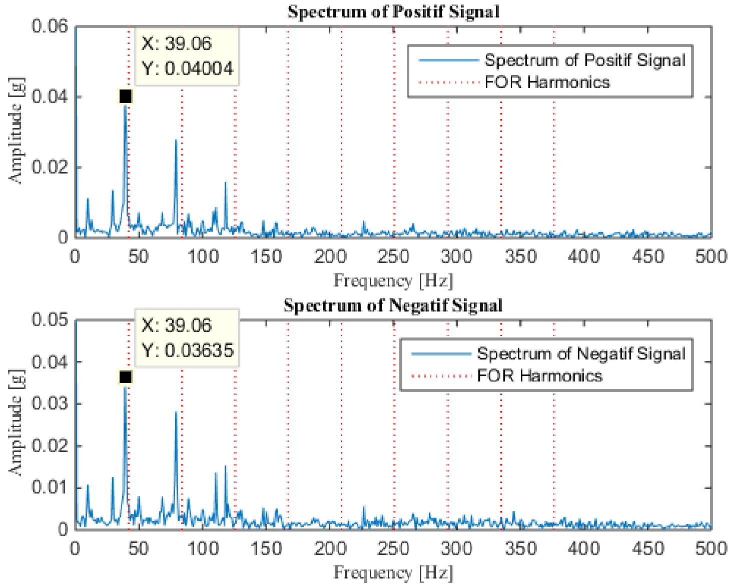

Figure 7

Spectrum of the positive and negative signals: outer ring defect detection

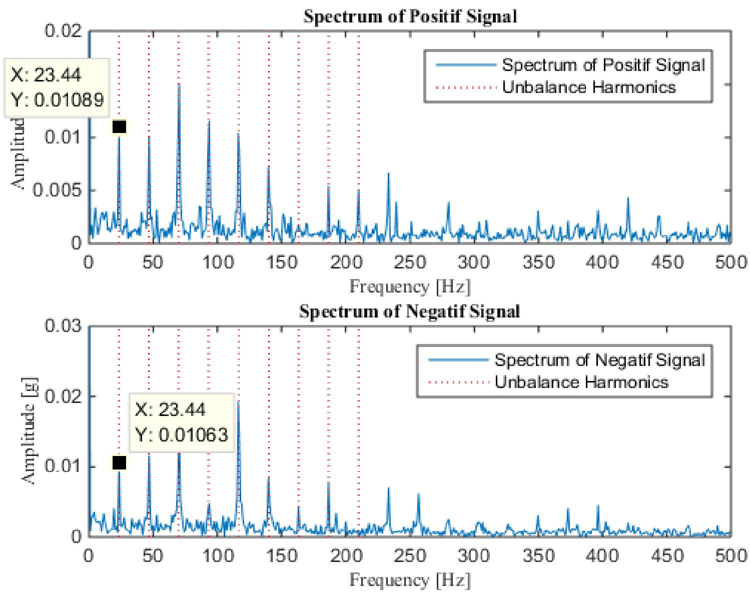

Figure 8

Spectrum of the positive and negative signals: rotor disk unbalance

5 Comparison of Diagnostic Methods

Yuhe Liao et al. proposed a method for diagnosing bearing faults. This method selects frequency bands with fault characteristics using multi-point kurtosis, which is used instead of spectral kurtosis to define the Kurtogram [28]. The proposed frequency band selection method, called the MKurtogram method, retains the same steps as the Kurtogram method but with a difference in the selection criteria [28]. Next, bandpass filtering is applied around the selected frequency interval, and then the envelope spectrum is determined to detect bearing faults [28]. Once this diagnostic method has been applied to the fault signal from the inner ring of the QJ212 TVP bearing, it will be analyzed using the proposed method (Fig.1) and presented in Table (2). The same result is achieved, as seen in figure (10), after filtering the signal around the central frequency of 3200 Hz within the band [0 Hz; 6400 Hz] at level (1), as specified by the MKurtogram in figure (9).

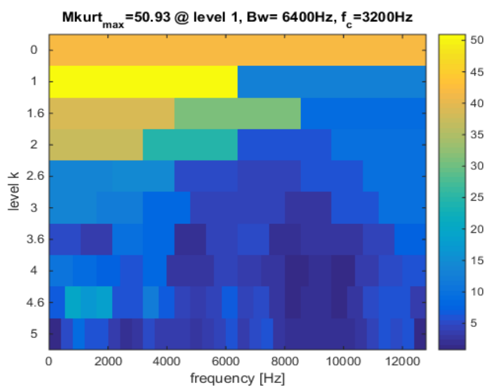

Figure 9

MKurtogram

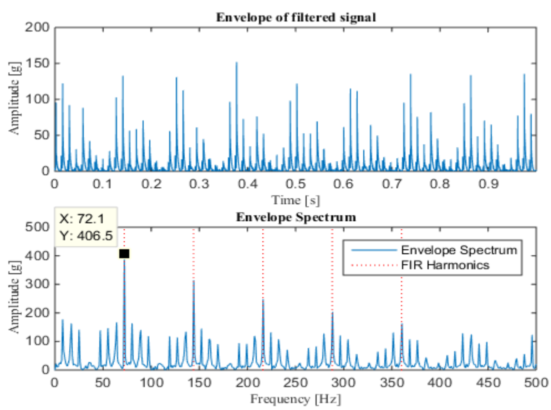

Figure 10

Envelope spectrum

Prashant Kumar Sahu et al. proposed a diagnostic method for the inner and outer ring defect signals of the 6205-SKF bearing, which is available in the Case Western Reserve University (CWRU) database [7]. The denoising diagnostic method comprises the following steps [7]:

- The signal was decomposed into several intrinsic mode functions using Complementary Ensemble Empirical Mode Decomposition (CEEMD), and the correlation between the raw signal and the functions was determined using the correlation coefficient. Functions representing correlation values between (0.5) and (0.9) were selected and denoised using adaptive thresholding.
- Reconstruction of the denoised signal, which is equal to the sum of the denoised functions and the functions expressing correlation values between (0.3) and (0.5).
- The envelope spectrum is determined to detect faults.

Once the proposed method (Fig.1) was applied to an inner ring fault signal, as shown in Table (4), a result identical to that obtained by the method of Sahu et al., was obtained, as shown in Figure (11).

Table 4

Inner ring fault signal

Signal	Speed [Rpm] and Load [Nm/s]	Defect diameter [mm]	Defect component	Fault frequency [Hz]	Sampling frequency [kHz]
111.mat	1750; 1491.38	0.1778	Inner race	157.9	48

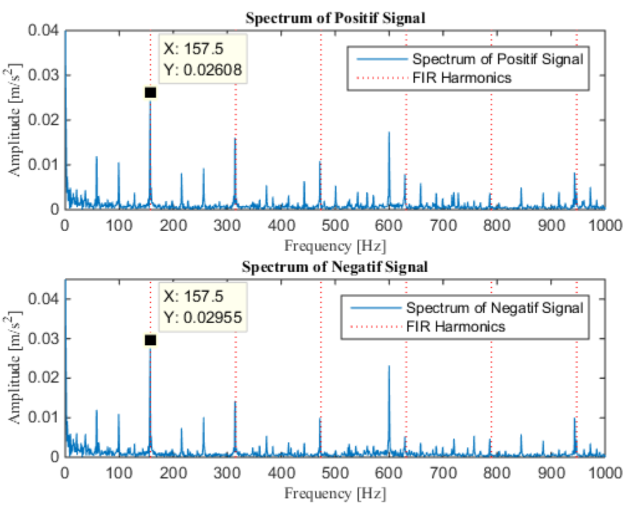

Figure 11

Inner ring fault detection

6 Conclusions

Five vibration signals corresponding to bearing defects were analyzed using the proposed detection method. According to these signals, good results were obtained, which were represented by strong peaks at the frequencies of the outer and inner rings and shaft unbalance defects. There is some variation between sparsity measurement indices. When only one index is used for defect data selection, mis-selection is possible. However, when several indexes are taken into account, differences between them are eliminated, and a large amount of defect information is collected. In addition, useless data not related to faults creates disturbances in the useful information, resulting in a complex shape of the spectrum. However, when this useless data is replaced by a series of zeros and useful data filtering is applied, the influence of noise is avoided.

The proposed positive and negative thresholding of the signals shows that the envelope determination does not rely solely on the Hilbert transform and the Teager-Kaiser energy operator. This thresholding, when used with Fourier transform as the final detection step, produces a shape very similar to that found in the envelope spectrum. When comparing diagnostic methods, there are differences in the way fault data are extracted. Each method incorporates a specific approach, such as denoising.

The approach used in the proposed method, based on signal segmentation, sparsity measurement and positive and negative thresholding, is effective because, the obtained results are identical to those provided by other diagnostic methods.

Nomenclature

Abbreviations

CMEEMD	Combined Modes Ensemble Empirical Mode Decomposition
DFA	Detrended Fluctuation Analysis
DS	Defect Symptom
EFD	Empirical Fourier Decomposition
FRE	Rolling element defect frequency
FC	Cage fault frequency
FIR	Inner ring fault frequency
FOR	Outer ring fault frequency
IMFs	Intrinsic Mode Functions
ISSA	Improved Singular Spectrum Analysis

IMED	Improved Minimum Entropy Deconvolution
KMAD	Kurtosis Median Absolute Deviation
MCKD	Maximum Correlation Kurtosis Deconvolution
SVMD	Successive Variational Mode Decomposition
SNR	Signal-to-Noise Ratio
VMD	Variational Mode Decomposition

Symbols

a	Contact angle	P_S	Positive thresholding
CC	Correlation coefficient	$S(f)$	Spectra of the positive and
Cov	Covariance	S_d	Dominant segment
D	Pitch diameter	S	Segments
d	Rolling element diameter	$TK[.]$	Taeger-Kaiser energy operator
E	Signal envelope	t	Time
f	Frequency	Var	Variance
Fr	Rotation speed	$W_{j,k}$	Wavelet transform coefficients
F_S	Sampling frequency	ψ	Mother wavelet
F_d	Fault frequency	$\overline{\psi}$	Conjugate complex of the mother
GE	Generalized envelope	x	Signal
$H[.]$	Hilbert transform	$\overline{x}$	Signal mean
M	Average signal	$\left\Vert \vec{x} \right\Vert_1$	L1 norm
N_S	Negative thresholding	$\dot{x}$ and	First and second derivatives of the
N	Signal length	Z	Series of zeros
NS	Number of segments	z	Number of rolling elements
N_p	Noise power	σ	Noise variance
S_p	Signal power	λ	Threshold

Acknowledgement

This work was supported by Electromechanical Engineering Laboratory.

References

[1] Du, Ying, et al. "Damage detection techniques for wind turbine blades: A review." Mechanical Systems and Signal Processing 141 (2020): 106445.

[2] Cheng, Jian, et al. "Adaptive periodic mode decomposition and its application in rolling bearing fault diagnosis." Mechanical Systems and Signal Processing 161 (2021): 107943.

[3] Li, Jimeng, et al. "Adaptive energy-constrained variational mode decomposition based on spectrum segmentation and its application in fault detection of rolling bearing." Signal Processing 183 (2021): 108025.

[4] Zhou, Wei, et al. "Empirical Fourier Decomposition: An Accurate Adaptive Signal Decomposition Method." arXiv preprint arXiv:2009.08047 (2020).

[5] Nazari, Mojtaba, and Sayed Mahmoud Sakhaei. "Successive variational mode decomposition." Signal Processing 174 (2020): 107610.

[6] Halidou, Aminou, et al. "Review of wavelet denoising algorithms." Multimedia Tools and Applications 82.27 (2023): 41539-41569.

[7] Sahu, Prashant Kumar, and Rajiv Nandan Rai. "Fault diagnosis of rolling bearing based on an improved denoising technique using complete ensemble empirical mode decomposition and adaptive thresholding method." Journal of Vibration Engineering & Technologies 11.2 (2023): 513-535.

[8] Li, Jin, Xian Zhang, and Jingtian Tang. "Noise suppression for magnetotelluric using variational mode decomposition and detrended fluctuation analysis." Journal of Applied Geophysics 180 (2020): 104127.

[9] Bouaouiche, Karim, Yamina Menasria, and Dalila Khalfa. "Diagnosis of rotating machine defects by vibration analysis." Acta IMEKO 12.1 (2023): 1-6.

[10] Miao, Yonghao, et al. "A review on the application of blind deconvolution in machinery fault diagnosis." Mechanical Systems and Signal Processing 163 (2022): 108202.

[11] Zhang, Zongzhen, et al. "Fast nonlinear blind deconvolution for rotating machinery fault diagnosis." Mechanical Systems and Signal Processing 187 (2023): 109918.

[12] Jain, Prashant H., and Santosh P. Bhosle. "A review on vibration signal analysis techniques used for detection of rolling element bearing defects." SSRG Int. J. Mech. Eng 8 (2021): 14-29.

[13] Moshrefzadeh, Ali, and Alessandro Fasana. "The Autogram: An effective approach for selecting the optimal demodulation band in rolling element bearings diagnosis." Mechanical systems and signal processing 105 (2018): 294-318.

[14] Medina, Rubén, et al. "Gear and bearing fault classification under different load and speed by using Poincaré plot features and SVM." Journal of Intelligent Manufacturing 33.4 (2022): 1031-1055.

[15] Zhou, Yuquan, and Chunxia Liu. "Bearing fault detection based on parameter adaptive variational modal decomposition and maximum correlation kurtosis deconvolution." Journal of Power Electronics 26.5 (2026): 1088-1102.

[16] Damine, Yasser, et al. "A new bearing fault detection strategy based on combined modes ensemble empirical mode decomposition, KMAD, and an enhanced deconvolution process." Energies 16.6 (2023): 2604.

[17] Xu, Zhi, Chaoren Qin, and Gang Tang. "A novel deconvolution cascaded variational mode decomposition for weak bearing fault detection with unknown signal transmission path." IEEE Sensors Journal 21.2 (2020): 1746-1755.

[18] Karim, Bouaouiche, et al. "Local Mean Decomposition, Using an Empirical Optimal Envelope and a Log-Envelope, for Bearing Fault Detection." Acta Polytechnica Hungarica, vol. 21, no. 4, 2024, pp. 265–80.

[19] Miao, Yonghao, Ming Zhao, and Jiadong Hua. "Research on sparsity indexes for fault diagnosis of rotating machinery." Measurement 158 (2020): 107733.

[20] Liu, Zhiwen, et al. "Abnormal detection gram (Andgram): An informative frequency band selection method using composite index for bearing incipient fault diagnosis." Mechanical Systems and Signal Processing 224 (2025): 112033.

[21] Albezzawy, Muhammad N., Mohamed G. Nassef, and Nader Sawalhi. "Rolling element bearing fault identification using a novel three-step adaptive and automated filtration scheme based on Gini index." ISA transactions 101 (2020): 453-460.

[22] Huimin, C. U. I., Zhao Ruimei, and H. O. U. Yanli. "Improved threshold denoising method based on wavelet transform." Physics procedia 33 (2012): 1354-1359.

[23] Jangjit, Sureewan, and Mahasak Ketcham. "A new wavelet denoising method for noise threshold." Engineering Journal 21.7 (2017): 141-155.

[24] Chen, Bingyan, et al. "Product envelope spectrum optimization-gram: An enhanced envelope analysis for rolling bearing fault diagnosis." Mechanical Systems and Signal Processing 193 (2023): 110270.

[25] Rodríguez, Patricia Henríquez, et al. "Application of the Teager–Kaiser energy operator in bearing fault diagnosis." ISA transactions 52.2 (2013): 278-284.

[26] Ismail, Mohamed AA, et al. "Ball bearing vibration data for detecting and quantifying spall faults." Data in Brief 47 (2023): 109019.

[27] Lee, Seongjae, Taewan Kim, and Taehyoun Kim. "Multi-domain vibration dataset with various bearing types under compound machine fault scenarios." Data in Brief 57 (2024): 110940.

[28] Liao, Yuhe, et al. "Extraction of repetitive transients with frequency domain multipoint kurtosis for bearing fault diagnosis." Measurement Science and Technology 29.5 (2018): 055012.